

Provable Guarantees for Understanding Out-of-distribution Detection

Peyman Morteza

Department of Computer Sciences
University of Wisconsin-Madison
peyman@cs.wisc.edu

Yixuan Li

Department of Computer Sciences
University of Wisconsin-Madison
sharonli@cs.wisc.edu

ABSTRACT

Out-of-distribution (OOD) detection is important for deploying machine learning models in the real world, where test data from shifted distributions can naturally arise. While a plethora of algorithmic approaches have recently emerged for OOD detection, a critical gap remains in theoretical understanding. In this work, we develop an analytical framework that characterizes and unifies the theoretical understanding for OOD detection. Our analytical framework motivates a novel OOD detection method for neural networks, *GEM*, which demonstrates both theoretical and empirical superiority. In particular, on CIFAR-100 as in-distribution data, our method outperforms a competitive baseline by 16.57% (FPR95). Lastly, we formally provide provable guarantees and comprehensive analysis of our method, underpinning how various properties of data distribution affect the performance of OOD detection¹.

1 Introduction

When deploying machine learning models in the open world, it becomes increasingly critical to ensure the reliability—models are not only accurate on their familiar data distribution, but also aware of unknown inputs outside the training data distribution. Out-of-distribution (OOD) samples can naturally arise from an irrelevant distribution whose label set has no intersection with training categories, and therefore should not be predicted by the model. This gives rise to the importance of OOD detection, which determines whether an input is in-distribution (ID) or OOD.

The main challenge in OOD detection stems from the fact that modern deep neural networks can easily produce overconfident predictions on OOD inputs [Nguyen et al., 2015]. This phenomenon makes the separation between ID and OOD data a non-trivial task. OOD detection approaches commonly rely on an OOD scoring function that derives statistics from the pre-trained neural networks and performs OOD detection by exercising a threshold comparison. For example, [Hendrycks and Gimpel, 2017] use the maximum softmax probability (MSP) and classifies inputs with smaller MSP scores as OOD data. While improved OOD scoring functions [Liang et al., 2018, Lee et al., 2018b, Liu et al., 2020, Sun et al., 2021] have emerged recently, their inherent connections and theoretical understandings are largely lacking. To the best of our knowledge, there is limited prior work providing provable guarantees for OOD detection methods from a rigorous mathematical point of view.

This paper takes an important step to bridge the gap by providing a unified framework that allows the research community to understand the theoretical connections among recent model-based OOD detection methods. Our framework further enables devising new methodology, theoretical and empirical insights on OOD detection. Our **key contributions** are three folds:

- First, we provide an analytical framework that precisely characterizes and unifies the theoretical interpretation of several representative OOD scoring functions (Section 2). We derive analytically an optimal form of OOD scoring function called *GEM* (*Gaussian mixture based Energy Measurement*), which is provably aligned with the true log-likelihood for capturing OOD uncertainty. In contrast, we show mathematically that prior scoring functions can be sub-optimal.
- Second, our analytical framework motivates a new OOD detection method for deep neural networks (Section 3). By modeling the feature space as a class-conditional multivariate Gaussian distribution, we propose a *GEM* score based on the Gaussian generative model. Empirical evaluations demonstrate the

¹Code is available at: <https://github.com/PeymanMorteza/GEM>

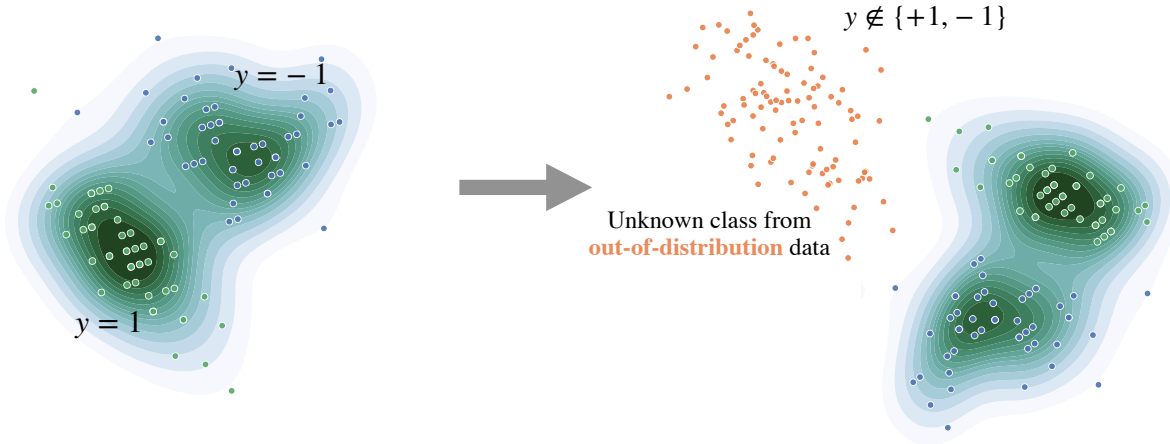


Figure 1.1: **Left:** The in-distribution data $P_{\mathcal{X}}^{\text{in}}$ comprises of two classes $\mathcal{Y} = \{-1, +1\}$, indicated by green and blue dots respectively. **Right:** Out-of-distribution detection allows the learner to express ignorance outside the support set of current known classes, and prevents the model from misclassifying OOD data (orange dots) into known classes (blue and green dots).

competitive performance of the new scoring function. In particular, on CIFAR-100 as in-distribution data, *GEM* outperforms [Liu et al., 2020] by 16.57% (FPR95). Our method is theoretically more rigorous than maximum Mahalanobis distance [Lee et al., 2018b] while achieving equally strong performance.

- Lastly, our work provides both provable guarantees and empirical analysis to understand how various properties of data representation in feature and input space affect the performance of OOD detection (Section 4). Previous OOD detection methods can be difficult to analyze due to the stochasticity in neural network optimization. Our framework offers key simplifications that allow us to (1) isolate the effect of data representation from model optimization, and (2) flexibly modulate properties of data representation in feature and input space. Through both synthetic simulations and theoretical analysis, our study reveals important insights on how OOD detection performance changes with respect to data distributions.

We end the introduction with an outline of this work. In Section 2, we first define the problem of study and set the notations that we need. Next, we analyze previous OOD detection methods under the Gaussian mixture assumption and introduce the GEM score. In Section 3, we extend GEM to deep neural networks and perform experiments on common benchmarks. In Section 4, we provide rigorous guarantees for the performance of GEM, along with simulation verifications. We conclude our work in Section 6, following an expansive literature review in Section 5.

2 OOD Detection Under Gaussian Mixtures

In this section, we mathematically describe representative OOD scoring functions under the Gaussian mixture data model. This allows us to contrast with the ideal OOD detector where the data density is explicit. We later apply the insight gained from this simple model to introduce a new score OOD detection for deep neural networks.

2.1 Preliminaries

We denote by $\mathcal{X} = \mathbb{R}^d$ the input space and $\mathcal{Y} = \{y_1, \dots, y_k\}$ the label space. Let $P_{\mathcal{X}, \mathcal{Y}}^{\text{in}}$ denote a probability distribution defined on $\mathcal{X} \times \mathcal{Y}$. Furthermore, let $P_{\mathcal{X}}^{\text{in}}$ and $P_{\mathcal{Y}}^{\text{in}}$ denote the marginal probability distribution on \mathcal{X} and \mathcal{Y} respectively. A classifier $f : \mathcal{X} \rightarrow \mathbb{R}^k$ learns to map a given input $\mathbf{x} \in \mathcal{X}$ to the output space.

Problem Statement Given a classifier f learned on training samples from in-distribution $P_{\mathcal{X}, \mathcal{Y}}^{\text{in}}$, the goal is to design a binary function estimator,

$$g : \mathcal{X} \rightarrow \{\text{in}, \text{out}\},$$

that classifies whether a test-time sample $\mathbf{x} \in \mathcal{X}$ is generated from $P_{\mathcal{X}}^{\text{in}}$ or not. Estimating OOD uncertainty is challenging due to the lack of knowledge on OOD data coming from $P_{\mathcal{X}}^{\text{out}}$. It is infeasible to explicitly train a

binary classifier g . A natural approach is to use level set for OOD detection, based on the data density $P_{\mathcal{X}}^{\text{in}}$. We define the *ideal classifier* for OOD detection as follows,

$$g_{\lambda}^{\text{ideal}}(\mathbf{x}) = \begin{cases} \text{in} & p_{\mathcal{X}}^{\text{in}}(\mathbf{x}) \geq \lambda \\ \text{out} & p_{\mathcal{X}}^{\text{in}}(\mathbf{x}) < \lambda \end{cases},$$

where $p_{\mathcal{X}}^{\text{in}}$ is the density function of $P_{\mathcal{X}}^{\text{in}}$ and λ is the threshold, which is chosen so that a high fraction (e.g., 95%) of in-distribution data is correctly classified. For evaluation purpose, we define the error rate by,

$$\begin{aligned} \text{TPR}(g) &:= \mathbb{E}_{\mathbf{x} \sim P_{\mathcal{X}}^{\text{in}}}(\mathbb{I}_{\{g(\mathbf{x})=\text{in}\}}), \\ \text{FPR}(g) &:= \mathbb{E}_{\mathbf{x} \sim P_{\mathcal{X}}^{\text{out}}}(\mathbb{I}_{\{g(\mathbf{x})=\text{in}\}}). \end{aligned}$$

By convention, we assume in-distribution samples have positive labels. In practice, $P_{\mathcal{X}}^{\text{out}}$ is often defined by a distribution that simulates unknowns encountered during deployment time, such as samples from an irrelevant distribution whose label set has no intersection with \mathcal{Y} and therefore should not be predicted by the model.

In-distribution Data Model We assume in-distribution data is drawn from a Gaussian mixture with equal priors and a tied covariance matrix Σ . The simplicity is desirable for us to precisely characterize various OOD detection methods and their optimality. We will further extend our analysis to neural networks in Section 3. Specifically,

$$\begin{aligned} \mathbf{x}|y_i &\sim \mathcal{N}(\boldsymbol{\mu}_i, \Sigma), \\ p_{\mathcal{Y}}^{\text{in}}(y_i) &= \frac{1}{k}, \end{aligned}$$

where $\boldsymbol{\mu}_i \in \mathbb{R}^d$ is the mean of class $y_i \in \mathcal{Y}$ and $\Sigma \in \mathbb{R}^{d \times d}$ is the covariance matrix. The class-conditional density follows a Gaussian distribution,

$$p_{\mathcal{X}|\mathcal{Y}}^{\text{in}}(\mathbf{x}|y_i) = \frac{1}{\sqrt{(2\pi)^d |\Sigma|}} \exp\left(-\frac{1}{2}(\mathbf{x} - \boldsymbol{\mu}_i)^{\top} \Sigma^{-1}(\mathbf{x} - \boldsymbol{\mu}_i)\right).$$

Above implies the density function of $P_{\mathcal{X}}^{\text{in}}$ can be written as follows,

$$\begin{aligned} p_{\mathcal{X}}^{\text{in}}(\mathbf{x}) &= \sum_{j=1}^k p_{\mathcal{X}|\mathcal{Y}}^{\text{in}}(\mathbf{x}|y_j) \cdot p_{\mathcal{Y}}^{\text{in}}(y_j) \\ &= \frac{1}{k \sqrt{(2\pi)^d |\Sigma|}} \sum_{j=1}^k \exp\left(-\frac{1}{2}(\mathbf{x} - \boldsymbol{\mu}_j)^{\top} \Sigma^{-1}(\mathbf{x} - \boldsymbol{\mu}_j)\right), \end{aligned}$$

which is mixture of k Gaussian distributions.

Bayes Optimal Classifier Under the Gaussian mixture model, the posterior probability of a Bayes optimal classifier for class $y_i \in \mathcal{Y}$ is given by,

$$p_{\mathcal{Y}|\mathcal{X}}(y_i|\mathbf{x}) = \frac{p_{\mathcal{Y}}(y_i) p_{\mathcal{X}|\mathcal{Y}}(\mathbf{x}|y_i)}{\sum_{j=1}^k p_{\mathcal{Y}}(y_j) p_{\mathcal{X}|\mathcal{Y}}(\mathbf{x}|y_j)} \quad (1)$$

$$= \frac{\exp\left(-\frac{1}{2}(\mathbf{x} - \boldsymbol{\mu}_i)^{\top} \Sigma^{-1}(\mathbf{x} - \boldsymbol{\mu}_i)\right)}{\sum_{j=1}^k \exp\left(-\frac{1}{2}(\mathbf{x} - \boldsymbol{\mu}_j)^{\top} \Sigma^{-1}(\mathbf{x} - \boldsymbol{\mu}_j)\right)} \quad (2)$$

$$= \frac{\exp f_i(\mathbf{x})}{\sum_{j=1}^k \exp f_j(\mathbf{x})}, \quad (3)$$

where $f : \mathcal{X} \rightarrow \mathbb{R}^k$ is a function mapping to the logits. One can note that the above form of posterior distribution is equivalent to applying the softmax function on the logits $f(\mathbf{x})$, where,

$$f_i(\mathbf{x}) = -\frac{1}{2}(\mathbf{x} - \boldsymbol{\mu}_i)^{\top} \Sigma^{-1}(\mathbf{x} - \boldsymbol{\mu}_i),$$

which is also known as the Mahalanobis distance [Mahalanobis, 1936].

2.2 OOD Scoring Functions and Their Optimality

We now contrast several representative OOD scoring functions and also introduce our new scoring function GEM. Note that an ideal OOD detector should use a scoring function that is proportional to the data density. We focus on post hoc OOD detection methods, which have the advantages of being easy to use and general applicability without modifying the training procedure and objective.

Prior: Maximum Softmax Score [Hendrycks and Gimpel](#) propose using the maximum softmax score (MSP) for estimating OOD uncertainty,

$$g_\lambda^{\text{MSP}}(\mathbf{x}) = \begin{cases} \text{in} & \text{MSP}(f, \mathbf{x}) \geq \lambda \\ \text{out} & \text{MSP}(f, \mathbf{x}) < \lambda \end{cases}.$$

The OOD scoring function is given by,

$$\begin{aligned} \text{MSP}(f, \mathbf{x}) &= \max_i p_{\mathcal{Y}|\mathcal{X}}(y_i|\mathbf{x}) \\ &= \max_i \frac{1}{k\beta p_{\mathcal{X}}^{\text{in}}(\mathbf{x})} \exp\left(-\frac{1}{2}(\mathbf{x} - \boldsymbol{\mu}_i)^\top \Sigma^{-1}(\mathbf{x} - \boldsymbol{\mu}_i)\right) \\ &\propto p_{\mathcal{X}}^{\text{in}}(\mathbf{x}), \end{aligned}$$

where $\beta = \sqrt{(2\pi)^d |\Sigma|}$. The above suggests that MSP is not aligned with the true data density, as illustrated in Figure 2.1. For simplicity, we visualize the case when the input distribution is mixture of one-dimensional Gaussians, with two classes $\mathcal{Y} = \{+1, -1\}$. MSP can yield high score 1, and misclassify data points in low-likelihood regions such as $x > 4$ or $x < -4$ (highlighted in red). Also, depending on threshold value λ , MSP may misclassify samples from neighbourhood around the origin (highlighted in gray).

Prior: Maximum Mahalanobis Distance [Lee et al.](#) propose using the maximum Mahalanobis distance *w.r.t* the closest class centroid for OOD detection. Specifically, the score is defined as:

$$\begin{aligned} M(f, \mathbf{x}) &= \max_i -(\mathbf{x} - \boldsymbol{\mu}_i)^\top \Sigma^{-1}(\mathbf{x} - \boldsymbol{\mu}_i) \\ &\propto p_{\mathcal{X}}^{\text{in}}(\mathbf{x}), \end{aligned}$$

which is equivalent to the maximum Mahalanobis distance. The corresponding OOD classifiers based on Mahalanobis score is,

$$g_\lambda^{\text{Mahalanobis}}(\mathbf{x}) = \begin{cases} \text{in} & M(f, \mathbf{x}) \geq \lambda \\ \text{out} & M(f, \mathbf{x}) < \lambda \end{cases}.$$

The above suggests that Mahalanobis distance is not proportional to the true data density either, hence sub-optimal.

Prior: Energy Score Given a function transformation $f : \mathcal{X} \rightarrow \mathbb{R}^k$, [Liu et al.](#) propose using the free energy score for OOD detection. The free energy is defined to be the $-\log \text{sumexp}$ of logit outputs,

$$E(f, \mathbf{x}) = -\log \sum_{j=1}^k \exp(f_j(\mathbf{x})), \quad (4)$$

where $f(\mathbf{x}) = (f_1(\mathbf{x}), \dots, f_k(\mathbf{x}))^\top \in \mathbb{R}^k$. We provide a simple and concrete example to show there exists maximum likelihood solution with the same posterior probability as in Equation 3, but the resulting energy score is not aligned with the data density:

$$\begin{aligned} p_{\mathcal{Y}|\mathcal{X}}(y_i|\mathbf{x}) &= \frac{\exp(-\frac{1}{2}(\mathbf{x} - \boldsymbol{\mu}_i)^\top \Sigma^{-1}(\mathbf{x} - \boldsymbol{\mu}_i))}{\sum_{j=1}^k \exp(-\frac{1}{2}(\mathbf{x} - \boldsymbol{\mu}_j)^\top \Sigma^{-1}(\mathbf{x} - \boldsymbol{\mu}_j))} \\ &= \frac{\exp(\boldsymbol{\mu}_i^\top \Sigma^{-1} \mathbf{x} - \frac{1}{2} \boldsymbol{\mu}_i^\top \Sigma^{-1} \boldsymbol{\mu}_i)}{\sum_{j=1}^k \exp(\boldsymbol{\mu}_j^\top \Sigma^{-1} \mathbf{x} - \frac{1}{2} \boldsymbol{\mu}_j^\top \Sigma^{-1} \boldsymbol{\mu}_j)} \\ &= \frac{\exp f'_i(\mathbf{x})}{\sum_{j=1}^k \exp f'_j(\mathbf{x})}, \end{aligned}$$

where $f'(\mathbf{x}) := (f'_1(\mathbf{x}), \dots, f'_k(\mathbf{x}))^\top \in \mathbb{R}^k$ can be viewed as a single layer network's output with (row) weights $\boldsymbol{\mu}_i^\top \Sigma^{-1}$, for $1 \leq i \leq k$, and biases $-\frac{1}{2} \boldsymbol{\mu}_i^\top \Sigma^{-1} \boldsymbol{\mu}_i$, for $1 \leq i \leq k$, and the corresponding energy $-\log \sum_j \exp f'_j(\mathbf{x})$ is not aligned with the log-likelihood, hence not always optimal.

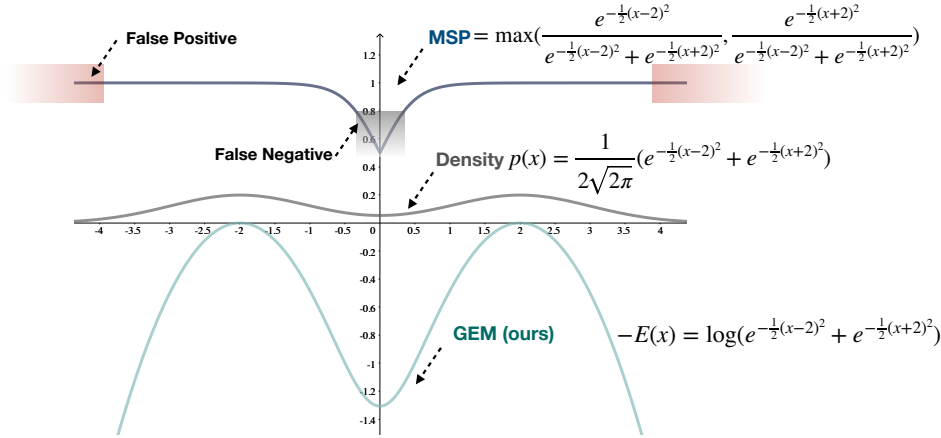


Figure 2.1: Illustration of data density (**middle**, gray), maximum softmax score (**top**, black) and GEM score (**bottom**, blue) when $x \in \mathbb{R}$. The data distribution $p(x)$ is a mixture of two Gaussians with mean $\mu_1 = 2$ and $\mu_2 = -2$ respectively. The variance $\sigma_1 = \sigma_2 = 1$. Under thresholding, MSP can not distinguish samples $x > 4$ or $x < -4$ which have low-likelihood of being in-distribution. In contrast, GEM score (ours) is aligned with the true data density, and better captures OOD uncertainty.

New: GEM Score We now introduce a new scoring function, Gaussian mixture based energy measurement (dubbed *GEM*). The GEM score can be written as,

$$\begin{aligned} \text{GEM}(f, \mathbf{x}) &= -E(f, \mathbf{x}) = \log \sum_{j=1}^k \exp\left(-\frac{1}{2}(\mathbf{x} - \boldsymbol{\mu}_j)^\top \Sigma^{-1}(\mathbf{x} - \boldsymbol{\mu}_j)\right) \\ &\propto \log p_{\mathcal{X}}^{\text{in}}(\mathbf{x}), \end{aligned}$$

which suggests that the *GEM score* is proportional (by ignoring a constant term) to the log-likelihood of the in-distribution data. Note that we flip the sign of free energy to align with the convention that larger GEM score indicates more ID-ness and vice versa. The key difference here is that the GEM score is a *special case* of negative free energy, where each $f_j(\mathbf{x})$ in Equation 4 takes on the form of Mahalanobis distance instead of directly using the logit outputs,

$$f_j(\mathbf{x}) = -\frac{1}{2}(\mathbf{x} - \boldsymbol{\mu}_j)^\top \Sigma^{-1}(\mathbf{x} - \boldsymbol{\mu}_j).$$

In Figure 2.1, we show the alignment between the GEM (light green) and true data density function (gray), in a simplified case with $x \in \mathbb{R}$, $k = 2$ and $\mu_1 = 2, \mu_2 = -2$. The corresponding OOD classifiers based on energy score is,

$$g_{\lambda}^{\text{GEM}}(\mathbf{x}) = \begin{cases} \text{in} & \text{GEM}(f, \mathbf{x}) \geq \lambda \\ \text{out} & \text{GEM}(f, \mathbf{x}) < \lambda \end{cases}.$$

This leads to the following lemma that shows the optimality of the GEM estimator.

Lemma 1. *In the case of Gaussian conditional with equal priors, the GEM based OOD estimator performs similarly to the ideal classifier defined in Section 2.1. More specifically,*

$$g_{\lambda}^{\text{ideal}} = g_{\log(k\beta \cdot \lambda)}^{\text{GEM}},$$

where $\beta = \sqrt{(2\pi)^d |\Sigma|}$ and both the ideal classifier and our method are aligned with $P_{\mathcal{X}}^{\text{in}}$ by definition.

Remark 1. Note that the equal prior case is considered to convey the main idea in simplest possible form. To make it more general, a weighted version of GEM can be used to achieve the optimality for the non-equal prior case. More precisely, let $w_i = p_{\mathbf{y}}^{\text{in}}(y_i)$, then we have,

$$\begin{aligned} p_{\mathcal{X}}^{\text{in}}(\mathbf{x}) &= \sum_{j=1}^k w_j p_{\mathcal{X}|Y}^{\text{in}}(\mathbf{x}|y_j) \\ &\propto \sum_{j=1}^k w_j \exp\left(-\frac{1}{2}(\mathbf{x} - \boldsymbol{\mu}_j)^\top \Sigma^{-1}(\mathbf{x} - \boldsymbol{\mu}_j)\right). \end{aligned}$$

Now if we define the *weighted GEM* by,

$$\text{GEM}^w(f, \mathbf{x}) := \log \sum_{j=1}^k w_j \exp\left(-\frac{1}{2}(\mathbf{x} - \boldsymbol{\mu}_j)^\top \Sigma^{-1}(\mathbf{x} - \boldsymbol{\mu}_j)\right),$$

then arguing similar to Lemma 1 implies that weighted GEM would be aligned with the ideal classifier in the non-equal prior case.

3 OOD Detection for Deep Neural Networks

In this section, we extend our analysis and method to deep neural networks. To start, let $h(\mathbf{x}; \theta) \in \mathbb{R}^m$ be the feature vector of the input \mathbf{x} , extracted from the penultimate layer of a neural net parameterized by θ . We assume that a class-conditional distribution in the feature space follows the multivariate Gaussian distribution. Such an assumption has been empirically validated in [Lee et al., 2018b]; also see visualizations in Figure 2.2. Specifically, a k class-conditional Gaussian distribution with a tied covariance is defined as,

$$h(\mathbf{x}; \theta) | y_i \sim \mathcal{N}(\mathbf{u}_i, \bar{\Sigma}),$$

where $\mathbf{u}_i \in \mathbb{R}^m$ is the mean of class y_i and $\bar{\Sigma} \in \mathbb{R}^{m \times m}$ is the covariance matrix. To estimate the parameters of the generative model from the pre-trained neural classifier, one can compute the empirical class mean and covariance given training samples $\{(\mathbf{x}_1, \bar{y}_1), (\mathbf{x}_2, \bar{y}_2), \dots, (\mathbf{x}_N, \bar{y}_N)\}$,

$$\hat{\mathbf{u}}_i = \frac{1}{N_i} \sum_{j: \bar{y}_j = y_i} h(\mathbf{x}_j; \theta),$$

$$\hat{\Sigma} = \frac{1}{N} \sum_{i=1}^k \sum_{j: \bar{y}_j = y_i} (h(\mathbf{x}_j; \theta) - \hat{\mathbf{u}}_i)(h(\mathbf{x}_j; \theta) - \hat{\mathbf{u}}_i)^T,$$

where N_i is the number of training samples with label $y_i \in \mathcal{Y}$. We can define the ideal classifier with respect to *feature space* to be,

$$g_\lambda^{\text{ideal}}(\mathbf{x}) = \begin{cases} \text{in} & p^{\text{feature}}(\mathbf{x}) \geq \lambda \\ \text{out} & p^{\text{feature}}(\mathbf{x}) < \lambda, \end{cases} \quad (5)$$

where p^{feature} denotes the density function of the posterior distribution on the feature space induced by $h(\mathbf{x}, \theta)$.

GEM for Neural Networks Similar to our definition in Section 2, *GEM* for neural networks can be defined as

$$\text{GEM}(\mathbf{x}; \theta) = \log \sum_{j=1}^k \exp(f_j(\mathbf{x}; \theta)),$$

where $f_j(\mathbf{x}; \theta) = -\frac{1}{2}(h(\mathbf{x}; \theta) - \mathbf{u}_j)^\top \bar{\Sigma}^{-1}(h(\mathbf{x}; \theta) - \mathbf{u}_j)$. We can empirically estimate each $f_j(\mathbf{x}; \theta)$ by,

$$\hat{f}_j(\mathbf{x}; \theta) = -\frac{1}{2}(h(\mathbf{x}; \theta) - \hat{\mathbf{u}}_j)^\top \hat{\Sigma}^{-1}(h(\mathbf{x}; \theta) - \hat{\mathbf{u}}_j).$$

It follows from an analogue of Lemma 1 that g_λ^{GEM} , computed from feature space, performs similarly to the ideal classifier that we defined by Equation 5.

Lemma 2. *The performance of GEM based detection is same as the ideal classifier (with respect to the feature space) defined by Equation 5 :*

$$g_\lambda^{\text{ideal}} = g_{\log(k\bar{\beta} \cdot \lambda)}^{\text{GEM}},$$

where $\bar{\beta} = \sqrt{(2\pi)^m |\bar{\Sigma}|}$.

We also note that Lemma 2 can be extended to non-equal prior case by arguing similar to Remark 1.

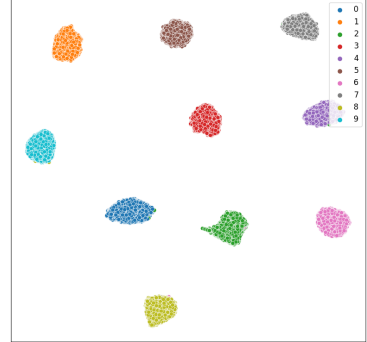


Figure 2.2: UMAP visualization of embeddings for CIFAR-10 model.

In-distribution	Method	FPR95	AUROC	AUPR	In-dist Test Error
		↓	↑	↑	↓
CIFAR-10	Softmax score [Hendrycks and Gimpel, 2017]	51.04	90.90	97.92	5.16
	ODIN [Liang et al., 2018]	35.71	91.09	97.62	5.16
	Mahalanobis [Lee et al., 2018b]	36.96	93.24	98.47	5.16
	Energy score [Liu et al., 2020]	33.01	91.88	97.83	5.16
	GEM (ours)	37.21	93.23	98.47	5.16
CIFAR-100	Softmax score [Hendrycks and Gimpel, 2017]	80.41	75.53	93.93	24.04
	ODIN [Liang et al., 2018]	74.64	77.43	94.23	24.04
	Mahalanobis [Lee et al., 2018b]	57.01	82.70	95.68	24.04
	Energy score [Liu et al., 2020]	73.60	79.56	94.87	24.04
	GEM (ours)	57.03	82.67	95.66	24.04

Table 1: **Main Results.** Comparison with competitive *post hoc* OOD detection methods. \uparrow indicates larger values are better, and \downarrow indicates smaller values are better. All values are percentages. Results for OOD detection are averaged over the six OOD test datasets described in section 3.1. Numbers for individual OOD test datasets are in the Appendix. The reported results for benchmarks other than GEM are courtesy of [Liu et al., 2020].

3.1 Experimental Results

Setup We use CIFAR-10 and CIFAR-100 [Krizhevsky et al., 2009] datasets as in-distribution data. We use the standard split, and train with WideResNet architecture [Zagoruyko and Komodakis, 2016] with depth 40. For the OOD test dataset, we use the following six datasets: Textures [Cimpoi et al., 2014], SVHN [Netzer et al., 2011], Places365 [Zhou et al., 2017], LSUN-Crop [Yu et al., 2015], LSUN-Resize [Yu et al., 2015], and iSUN [Xu et al., 2015]. We report standard metrics including FPR95 (false positive rate of OOD examples when the true positive rate of in-distribution examples is at 95%), AUROC, and AUPR.

GEM is both empirically competitive and theoretically grounded. Table 1 compares the performance of the GEM method with common OOD detection methods. For fairness, all methods derive OOD scoring functions *post hoc* from the same pre-trained model. For example, on CIFAR-100 as in-distribution data, GEM outperforms the energy score [Liu et al., 2020] by 16.57% (FPR95). Compared to [Lee et al., 2018b], our method is more theoretically grounded than taking the maximum Mahalanobis distance. We note that the similar empirical performance is primarily due to \log -sum-exp being a smooth approximation of maximum Mahalanobis distance in the feature space (more details in Remark 2 below). Therefore, our method overall achieves both strong empirical performance and theoretical soundness—bridging a critical gap under unified understandings.

3.2 Remarks

Remark 2 (Significance *w.r.t* Mahalanobis). The main difference *w.r.t* [Lee et al., 2018b] is that we are taking the \log -sum-exp over Mahalanobis distances M_i , instead of taking the maximum Mahalanobis distance. This was motivated by our theoretical analysis in previous Section where taking \log -sum-exp would be aligned with likelihood (*w.r.t* feature space), whereas \max is not exact in theory. In other words, we bring theoretical rigor to an empirically competitive method. Mathematically, $\log \sum_i^k \exp(M_i) \approx \max_i M_i$ with the following bound: $\max_i M_i \leq \log \sum_i^k \exp(M_i) \leq \max_i M_i + \log(k)$. Therefore, our method overall achieves equally strong empirical performance yet with theoretical soundness and guarantees (see formal analysis in Section 4).

Lemma 3. *In the case of Gaussian conditional with equal priors in the feature space, the Mahalanobis-based OOD estimator is not aligned with the density of in-distribution data in the feature space and it is not equivalent to the ideal classifier defined by Equation 5.*

Remark 3 (Significance *w.r.t* Energy Score). The energy score in [Liu et al., 2020] was derived directly from the logit outputs, rather than a Gaussian generative model as in ours. As a result, the original energy score might not always correspond to the Bayes optimal logit to ensure alignment *w.r.t* likelihood (we showed this by an explicit example in Section 2). Instead, our analytical framework and method provide strong provable guarantees (c.f. Section 4) and enable precise understanding by disentangling the effects of various factors (c.f. Section 4), both of which were not presented in [Liu et al., 2020]. Moreover, we show empirically that GEM achieves strong empirical performance, outperforming energy score by a significant margin (16.57% in FPR95 on CIFAR-100, see Table 1).

4 Provable Guarantees for GEM

The main goal of this section is to provide rigorous guarantees and understandings for our method GEM. This is important but often missing in previous literature on OOD detection.

Let $P_{\mathcal{X}}^{\text{in}}$ be a mixture of Gaussians (similar to Section 2) and assume $P_{\mathcal{X}}^{\text{out}} = \mathcal{N}(\boldsymbol{\mu}_{\text{out}}, \Sigma)$. We can think of \mathcal{X} as either the feature space or input space of a deep neural net. We work with the re-scaled version of the GEM score (by omitting the log operator), which does not change the formal guarantees.

$$ES(\mathbf{x}) = \sum_{i=1}^k ES_i(\mathbf{x}),$$

where,

$$ES_i(\mathbf{x}) = \exp\left(-\frac{1}{2}(\mathbf{x} - \boldsymbol{\mu}_i)^\top \Sigma^{-1}(\mathbf{x} - \boldsymbol{\mu}_i)\right).$$

Next, we consider the following quantity,

$$D := \mathbb{E}_{\mathbf{x} \sim P_{\mathcal{X}}^{\text{in}}}(ES(\mathbf{x})) - \mathbb{E}_{\mathbf{x} \sim P_{\mathcal{X}}^{\text{out}}}(ES(\mathbf{x})).$$

Intuitively, we can think of D as a measure of how well GEM distinguishes ID samples from OOD samples. For example, when $\boldsymbol{\mu}_{\text{out}}$ is far away from $\boldsymbol{\mu}_i$ then we expect $\mathbb{E}_{\mathbf{x} \sim P_{\mathcal{X}}^{\text{out}}}(ES(\mathbf{x}))$ to be small (i.e., D is large), and we expect that the our OOD estimator performs better compared to the case when $\boldsymbol{\mu}_{\text{out}}$ is close to $\boldsymbol{\mu}_i$ (i.e., D is small). We make this intuition precise by bounding D in terms of Mahalanobis distance between $\boldsymbol{\mu}_{\text{out}}$ and $\boldsymbol{\mu}_i$. First, we recall the following definition and set some notations,

Definition 1. For $\mathbf{u}, \mathbf{v} \in \mathbb{R}^d$, the Mahalanobis distance, with respect to Σ , is defined by,

$$d_M(\mathbf{u}, \mathbf{v}) := \sqrt{(\mathbf{u} - \mathbf{v})^\top \Sigma^{-1}(\mathbf{u} - \mathbf{v})},$$

and for $r > 0$ the open ball with center \mathbf{u} and radius r is defined by,

$$B_r(\mathbf{u}) := \{\mathbf{x} \in \mathbb{R}^d \mid d_M(\mathbf{x}, \mathbf{u}) < r\}.$$

Next, we can state the following theorem.

Theorem 1. We have the following bounds,

- $\mathbb{E}_{\mathbf{x} \sim P_{\mathcal{X}}^{\text{out}}}(ES(\mathbf{x})) \leq \sum_{i=1}^k \left((1 - P_{\mathcal{X}}^{\text{out}}(B_{\alpha_i}(\boldsymbol{\mu}_{\text{out}}))) + \exp(-\frac{1}{2}\alpha_i^2) \right),$
- $\mathbb{E}_{\mathbf{x} \sim P_{\mathcal{X}}^{\text{in}}}(ES(\mathbf{x})) - \mathbb{E}_{\mathbf{x} \sim P_{\mathcal{X}}^{\text{out}}}(ES(\mathbf{x})) \leq \sum_{i=1}^k \alpha_i,$

where, for $1 \leq i \leq k$, $\alpha_i := \frac{1}{2}d_M(\boldsymbol{\mu}_i, \boldsymbol{\mu}_{\text{out}})$.

We emphasize that in Theorem 1 $\boldsymbol{\mu}_i$ and $\boldsymbol{\mu}_{\text{out}}$ can have arbitrary configurations. We refer the reader to the Appendix for the proof of Theorem 1 and detailed discussions on other variants.

Performance with respect to the distance between ID and OOD data The next corollary explains how Theorem 1 can quantify that the performance of GEM-based OOD detector increases as the distance between ID and OOD data increases.

Corollary 1. For $1 \leq i \leq k$, set $\alpha = d_M(\boldsymbol{\mu}_{\text{out}}, \boldsymbol{\mu}_i)$. We have the following from the first bound in Theorem 1,

$$\mathbb{E}_{\mathbf{x} \sim P_{\mathcal{X}}^{\text{out}}}(ES(\mathbf{x})) \leq k \left((1 - P_{\mathcal{X}}^{\text{out}}(B_{\alpha}(\boldsymbol{\mu}_{\text{out}}))) + \exp(-\frac{1}{2}\alpha^2) \right).$$

Now as $\alpha \rightarrow \infty$ the right hand side in the above approaches to 0. This indicates that the performance of our method improves as $\alpha \rightarrow \infty$. On the other hand, using the second bound in the Theorem 1, we have,

$$\mathbb{E}_{\mathbf{x} \sim P_{\mathcal{X}}^{\text{in}}}(ES(\mathbf{x})) - \mathbb{E}_{\mathbf{x} \sim P_{\mathcal{X}}^{\text{out}}}(ES(\mathbf{x})) \leq k\alpha,$$

and it follows that as $\alpha \rightarrow 0$ the energy difference between in-distribution and out-of-distribution data converges to 0. In other words, the performance decreases as α approaches to 0. We will further justify our theory in simulation study (next subsection).

Performance in high dimensions We now show that the performance of GEM decreases as dimension of feature space increases. This is due to *curse of dimensionality* which we next explain. First, for simplicity assume that $\boldsymbol{\mu}_{out} = \mathbf{0}$ and for all $1 \leq i \leq k$, $\alpha = d_M(\boldsymbol{\mu}_{out}, \boldsymbol{\mu}_i)$. Consider a multi-dimensional gaussian $\mathcal{N}(0, \mathbf{I}_d)$. As d increases the high-probability region under this gaussian distribution will concentrate away from the origin. More precisely,

$$\mathbf{x} \sim \mathcal{N}(0, \mathbf{I}_d) \implies \|\mathbf{x}\|_2^2 \sim \chi_d^2 \implies \mathbb{E}(\|\mathbf{x}\|_2^2) = d.$$

Therefore, the out-of-distribution samples will have a larger distance (on average) to the origin as dimension increases and it follows that the OOD detector may misclassify these OOD samples as in-distribution.

We next conduct several simulation studies to systematically verify our provable guarantees.

4.1 Simulation Studies and Further Analysis

What properties of the data representation make OOD uncertainty challenging? In this subsection, we construct a synthetic data representation that allows us to flexibly modulate different properties of the data representation including:

- (i) distance between ID and OOD data,
- (ii) feature or input dimension,
- (iii) number of classes.

We simulate and probe how these factors affect OOD uncertainty estimation. The simulation also serves as a verification of our theoretical guarantees.

Feature representation setup The in-distribution representation on the feature space (or input space) comprises a mixture of k class-conditional Gaussian. To replicate common empirical benchmarks such as CIFAR-10 and CIFAR-100 [Krizhevsky et al., 2009], we explore both $k = 10$ and $k = 100$ by default. Unless otherwise specified, we set the feature (or input) dimension $d = 512$. We fix the total number of in-distribution samples $N = 20,000$. The tied covariance matrix is diagonal with magnitude σ^2 , i.e., $\Sigma = \sigma^2 \mathbf{I}_d$.

We assume the data in the feature space (or input space) $\mathbf{x} \in \mathbb{R}^d$ is sampled from the following class-conditional Gaussian,

$$\mathbf{x}_{in} | y_i \sim \mathcal{N}(\boldsymbol{\mu}_i, \sigma^2 \mathbf{I}_d),$$

where $\boldsymbol{\mu}_i$ is the mean for in-distribution classes $i \in \{1, 2, \dots, k\}$. We consider different configurations of $\boldsymbol{\mu}_i$, $1 \leq i \leq k$ representing means of each k in-distribution classes. Specifically, the mean $\boldsymbol{\mu}_i$ corresponding to i -th class is a unit vector \boldsymbol{v}_i , scaled by a distance parameter $r > 0$. In particular, $\boldsymbol{\mu}_i = r \cdot \boldsymbol{v}_i$, where $\|\boldsymbol{v}_i\|_2 = 1$. \boldsymbol{v}_i is a sparse vector with $s = \lfloor d/k \rfloor$ non-zero entries, with equal values in the position from $(i-1) \cdot s$ up to $i \cdot s$ and 0 elsewhere. It follows that for $i, j \in \{1, \dots, k\}$ and $i \neq j$,

$$\begin{aligned} \langle \boldsymbol{v}_i, \boldsymbol{v}_j \rangle &= 0, \\ \|\boldsymbol{v}_i - \boldsymbol{v}_j\|_2 &= \sqrt{2}. \end{aligned} \tag{6}$$

Furthermore, we assume that the out-of-distribution data representation is centered at the origin, with $\boldsymbol{\mu}_{out} = \mathbf{0} \in \mathbb{R}^d$,

$$\mathbf{x}_{out} \sim \mathcal{N}(\mathbf{0}, \sigma^2 \mathbf{I}_d).$$

Note that the above configuration is considered for simplicity and similar simulation results holds when we translate $\boldsymbol{\mu}_i$ and $\boldsymbol{\mu}_{out}$ with a constant vector or by applying an orthogonal transformation.

Rationale of the synthetic data Compared to estimating GEM scores from real datasets using parameterized models (such as neural networks), these synthetic simulations offer two key simplifications. First, viewing the setting on feature space, we can *flexibly modulate* key properties of datasets such as the number of classes and distance between induced ID and OOD representation in the feature space. In contrast, in real datasets, these properties are usually predetermined. Second, viewing the setting on input space, the function mapping $f(\mathbf{x})$ is completely deterministic and optimal, provided with known parameters $\{\boldsymbol{\mu}_1, \boldsymbol{\mu}_2, \dots, \boldsymbol{\mu}_k\}$ and Σ . This allows us to isolate the effect of data distribution from model optimization. In contrast, estimating $f(\mathbf{x})$ using complex models such as neural networks might have inductive bias, and depend on the optimization algorithm chosen.

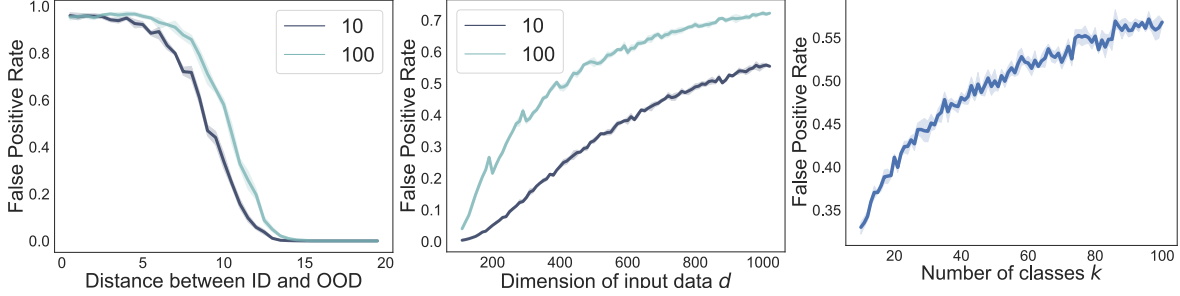


Figure 4.1: distance between ID and OOD (**left**), the dimension of input data d (**middle**), and number of classes (**right**). Each curve is averaged over 5 different runs (shade indicates the variance). A lower value on the y-axis is better. The covariance matrix Σ is set to be identity in all of these simulations.

Performance with respect to the number of classes We now show that the performance of our method decreases as the number of classes increases. To explain this, we compute D in terms of k to see how they are related. First, we need the following definition,

Definition 2. Let $\mu, \nu \in \mathbb{R}^d$ with $\gamma = \|\mu - \nu\|_2$. Let $P \sim \mathcal{N}(\mu, \mathbf{I}_d)$. Define,

$$A_\gamma := \mathbb{E}_{\mathbf{x} \sim P}(\exp(-\frac{1}{2} \|\mathbf{x} - \nu\|_2^2)).$$

Remark 4. Notice that, since standard Gaussian distribution is rotationally invariant, A_γ only depends on the distance between μ and ν (i.e. γ). Also it is easy to see that A_γ decreases as γ increases.

Proposition 2. We have the following,

$$D = A_0 - A_r + (k - 1)(A_{\sqrt{2} \cdot r} - A_r).$$

We refer the reader to the Appendix for the proof of Proposition 2. The next Corollary explains how the performance of our method decreases by increasing the number of classes.

Corollary 2. Since $\sqrt{2} \cdot r > r$, it follows from Remark 4 that $A_{\sqrt{2} \cdot r} < A_r$. This means that the last term in the following is negative,

$$D = A_0 - A_r + (k - 1)(A_{\sqrt{2} \cdot r} - A_r).$$

In other words, as k increases D becomes smaller which indicates that the performance of the GEM method decreases.

4.2 Simulation Results

In this subsection, we report simulation results that confirm our theoretical guarantees presented above.

Effect of distance between ID and OOD Figure 4.1 (left) shows how the False Positive Rate (at 95% TPR) changes with the distance between ID and OOD features. The σ is set to be 1 and the distance is modulated by adjusting the magnitude parameter r , where a larger r results in a larger distance. For both $k = 10$ and $k = 100$, the FPR decreases as the distance increases, which matches our intuition that more drastic distribution shifts are easier to be detected. Under the same distance, we observe a relatively higher FPR for data with more classes ($k = 100$). The performance gap diminishes as the distance becomes very large.

Higher dimension exacerbates OOD uncertainty Figure 4.1 (middle) shows how the FPR changes as we increase the input dimension from $d = 100$ to $d = 1,000$ while keeping the distance fixed with $r = 10$ and $\sigma = 1$. As the dimension d increases, the number of non-zero entries in each μ_i increases accordingly (i.e. μ_i becomes less sparse). Under the same feature dimension, we observe a higher FPR for $k = 100$ than $k = 10$, which corroborates the empirical observations on CIFAR-10 and CIFAR-100 (Section 3.1). This suggests that higher dimensions can be a key factor inducing the detrimental effect in OOD detection.

Effect of the number of classes Lastly, we investigate the performance of OOD uncertainty estimation by linearly increasing the number of classes k from 10 to 100. We keep the magnitude parameter fixed with $r = 10$ and dimension $d = 512$ and $\sigma = 1$. We see as the number of classes increases, the performance of our method decreases. We close this section by noting that we also provided formal mathematical justifications in the previous subsection.

5 Related Work

Detecting unknowns has a long history in machine learning. We review works that are studied this problem in the context of deep neural networks. See [Yang et al., 2021] for a survey on generalized OOD detection (an umbrella term that includes closely related domains such as anomaly detection, novelty detection, open-set recognition, and OOD detection).

Out-of-distribution detection for discriminative models In [Bendale and Boult, 2015], the OpenMax score is developed for OOD detection based on the extreme value theory (EVT). Subsequent work by Hendrycks and Gimpel proposed a simple baseline using maximum softmax probability. The MSP score for OOD input is proven to be arbitrarily high for neural networks with ReLU activation [Hein et al., 2019]. Liang et al. improved MSP by proposing the ODIN score, which amplifies the ID and OOD separability. It is shown that a sufficiently large temperature has a strong smoothing effect that transforms the softmax score back to the logit space—which more effectively distinguishes between ID vs. OOD. In [Lee et al., 2018b], a score is constructed based on the maximum Mahalanobis distance to the class means in the feature space of the pre-trained network. Liu et al., proposed using the energy score, which can be derived directly from the logit output of the pre-trained network. In [Huang and Li, 2021], OOD detection is studied when the label space is large. It is shown that grouping the labels for in-distribution data can be effective in OOD detection for large semantic space. In [Ming et al., 2022], the effect of spurious correlation is studied for OOD detection. Huang et al. derived a scoring function termed GradNorm from the gradient space. GradNorm employs the vector norm of gradients, backpropagated from the KL divergence between the softmax output and a uniform probability distribution. In [Wang et al., 2021], the OOD detection is studied for multi-label classification where each data instance has multiple labels. In this work, we develop an analytical framework to analyze the performance of OOD scoring functions and show the superiority of GEM both theoretically and empirically.

Out-of-distribution detection via generative modeling There are several works that attempt modeling OOD data using generative modeling (e.g. GANs). Lee et al. use GANs to generate data with low density for model regularization. Vernekar et al. model in-distribution as a low dimensional submanifold of input space and uses auto-encoders to generate OOD samples outside of the in-distribution domain. Sricharan and Srivastava use GANs to generate OOD samples that the initial classifier is confident about and use those to create a more robust OOD detector. Prior research also used generative modeling to estimate the density of the in-distribution data, and classify a sample as OOD if the estimated likelihood is low. However, it is shown in [Nalisnick et al., 2019] that deep generative models can produce a higher likelihood for OOD data. For example, it fails to distinguish CIFAR10 samples from SVHN. In [Ren et al., 2019] and [Serrà et al., 2020], this problem is addressed by considering a likelihood ratio and taking the input complexity into account.

Out-of-distribution detection by model regularization Several works address the out-of-distribution detection problem during training-time regularization [Lee et al., 2018a, Bevandić et al., 2018, Geifman and El-Yaniv, 2019, Malinin and Gales, 2018b, Mohseni et al., 2020, Jeong and Kim, 2020, Chen et al., 2021]. In [Lee et al., 2018a], a new term is added to the loss function of the neural net to force the out-of-distribution sample to have uniform prediction values across labels. A similar loss is followed by outlier exposure [Hendrycks et al., 2018]. In [Liu et al., 2020], a term is added to the loss function of the network to force out-distribution samples to have higher energy values after training. In [Chen et al., 2021], an informative outlier mining procedure is proposed, which adaptively samples from auxiliary OOD data that is near the decision boundary between ID and OOD.

Such methods typically require having access to auxiliary unlabeled data. We focus on post hoc OOD detection methods, which have the advantages of being easy to use and general applicability. This is convenient for the adoption of OOD detection methods in real-world production environments, where the overhead cost of retraining or modifying the model can be prohibitive.

Uncertainty estimation in deep neural networks A Bayesian model is a statistical model that implements Bayes’ rule to infer uncertainty within the model [Jaynes, 1986]. Recent works attempt several approximations of Bayesian inference including MC-dropout [Gal and Ghahramani, 2016] and deep ensembles [Dietterich, 2000, Lakshminarayanan et al., 2017]. These methods address model uncertainty (*i.e.*, epistemic) and are less competitive for OOD uncertainty estimation. Kendall and Gal developed an extended framework to study aleatoric and epistemic uncertainty together. In [Van Amersfoort et al., 2020] an uncertainty estimation method is developed using the RBF network. Dirichlet Prior Network (DPN) is also used for OOD detection with an uncertainty modeling of three different sources of uncertainty: model uncertainty, data uncertainty, and distributional uncertainty and form a line of works [Malinin and Gales, 2018a, 2019, Nandy et al., 2020].

6 Conclusion

In this work, we develop an analytical framework that precisely characterizes and unifies the theoretical understanding of out-of-distribution detection. Our analytical framework motivates a novel OOD detection method for neural networks, *GEM*, which demonstrates both theoretical and empirical superiority. We formally provide provable guarantees and comprehensive analysis of our method, underpinning how various properties of data distribution affect the performance of OOD detection. We hope our work can motivate future research on the theoretical understandings of OOD detection.

Acknowledgment

The authors would like to thank Yifei Ming for the helpful discussion. This work is supported by the Wisconsin Alumni Research Foundation (WARF). YL is also supported by the Facebook Research Award, JP Morgan faculty award, and funding from Google Brain and American Family Insurance.

References

- Abhijit Bendale and Terrance Boult. Towards open world recognition. In *Proceedings of the IEEE conference on computer vision and pattern recognition*, pages 1893–1902, 2015.
- Petra Bevandić, Ivan Krešo, Marin Oršić, and Siniša Šegvić. Discriminative out-of-distribution detection for semantic segmentation. *arXiv preprint arXiv:1808.07703*, 2018.
- Jiefeng Chen, Yixuan Li, Xi Wu, Yingyu Liang, and Somesh Jha. Atom: Robustifying out-of-distribution detection using outlier mining. In *Proceedings of European Conference on Machine Learning and Principles and Practice of Knowledge Discovery in Databases (ECML PKDD)*, 2021.
- Mircea Cimpoi, Subhransu Maji, Iasonas Kokkinos, Sammy Mohamed, and Andrea Vedaldi. Describing textures in the wild. In *Proceedings of the IEEE Conference on Computer Vision and Pattern Recognition*, pages 3606–3613, 2014.
- Thomas G Dietterich. Ensemble methods in machine learning. In *International workshop on multiple classifier systems*, 2000.
- Yarin Gal and Zoubin Ghahramani. Dropout as a bayesian approximation: Representing model uncertainty in deep learning. In *ICML*, 2016.
- Yonatan Geifman and Ran El-Yaniv. Selectivenet: A deep neural network with an integrated reject option. *arXiv preprint arXiv:1901.09192*, 2019.
- Matthias Hein, Maksym Andriushchenko, and Julian Bitterwolf. Why relu networks yield high-confidence predictions far away from the training data and how to mitigate the problem. In *Proceedings of the IEEE Conference on Computer Vision and Pattern Recognition*, pages 41–50, 2019.
- Dan Hendrycks and Kevin Gimpel. A baseline for detecting misclassified and out-of-distribution examples in neural networks. *Proceedings of International Conference on Learning Representations*, 2017.
- Dan Hendrycks, Mantas Mazeika, and Thomas Dietterich. Deep anomaly detection with outlier exposure. *arXiv preprint arXiv:1812.04606*, 2018.
- Rui Huang and Yixuan Li. Mos: Towards scaling out-of-distribution detection for large semantic space. In *Proceedings of the IEEE/CVF Conference on Computer Vision and Pattern Recognition*, pages 8710–8719, 2021.
- Rui Huang, Andrew Geng, and Yixuan Li. On the importance of gradients for detecting distributional shifts in the wild. *Neural Information Processing Systems*, 2021.
- Edwin T Jaynes. Bayesian methods: General background. 1986.
- Taewon Jeong and Heeyoung Kim. Ood-maml: Meta-learning for few-shot out-of-distribution detection and classification. *Advances in Neural Information Processing Systems*, 33, 2020.
- Alex Kendall and Yarin Gal. What uncertainties do we need in bayesian deep learning for computer vision? In *Advances in neural information processing systems*, pages 5574–5584, 2017.
- Alex Krizhevsky, Geoffrey Hinton, et al. Learning multiple layers of features from tiny images. 2009.
- Balaji Lakshminarayanan, Alexander Pritzel, and Charles Blundell. Simple and scalable predictive uncertainty estimation using deep ensembles. *NeurIPS*, 2017.

- Kimin Lee, Honglak Lee, Kibok Lee, and Jinwoo Shin. Training confidence-calibrated classifiers for detecting out-of-distribution samples. *Proceedings of the International Conference on Learning Representations*, 2018a.
- Kimin Lee, Kibok Lee, Honglak Lee, and Jinwoo Shin. A simple unified framework for detecting out-of-distribution samples and adversarial attacks. In *Advances in Neural Information Processing Systems*, pages 7167–7177, 2018b.
- Shiyu Liang, Yixuan Li, and Rayadurgam Srikant. Enhancing the reliability of out-of-distribution image detection in neural networks. In *6th International Conference on Learning Representations, ICLR 2018*, 2018.
- Weitang Liu, Xiaoyun Wang, John Owens, and Yixuan Li. Energy-based out-of-distribution detection. *Advances in Neural Information Processing Systems*, 2020.
- Prasanta Chandra Mahalanobis. On the generalized distance in statistics. National Institute of Science of India, 1936.
- Andrey Malinin and Mark Gales. Predictive uncertainty estimation via prior networks. In *NeurIPS*, 2018a.
- Andrey Malinin and Mark Gales. Predictive uncertainty estimation via prior networks. In *Advances in Neural Information Processing Systems*, pages 7047–7058, 2018b.
- Andrey Malinin and Mark Gales. Reverse kl-divergence training of prior networks: Improved uncertainty and adversarial robustness. In *NeurIPS*, 2019.
- Yifei Ming, Hang Yin, and Yixuan Li. On the impact of spurious correlation for out-of-distribution detection. *Proceedings of the AAAI Conference on Artificial Intelligence*, 2022.
- Sina Mohseni, Mandar Pitale, JBS Yadawa, and Zhangyang Wang. Self-supervised learning for generalizable out-of-distribution detection. In *AAAI*, pages 5216–5223, 2020.
- Alfred Müller. Integral probability metrics and their generating classes of functions. *Advances in Applied Probability*, pages 429–443, 1997.
- Eric Nalisnick, Akihiro Matsukawa, Yee Whye Teh, Dilan Gorur, and Balaji Lakshminarayanan. Do deep generative models know what they don’t know? *International Conference on Learning Representations*, 2019.
- Jay Nandy, Wynne Hsu, and Mong Li Lee. Towards maximizing the representation gap between in-domain & out-of-distribution examples. In *NeurIPS*, 2020.
- Yuval Netzer, Tao Wang, Adam Coates, Alessandro Bissacco, Bo Wu, and Andrew Y Ng. Reading digits in natural images with unsupervised feature learning. 2011.
- Anh Nguyen, Jason Yosinski, and Jeff Clune. Deep neural networks are easily fooled: High confidence predictions for unrecognizable images. In *Proceedings of the IEEE conference on computer vision and pattern recognition*, pages 427–436, 2015.
- Jie Ren, Peter J Liu, Emily Fertig, Jasper Snoek, Ryan Poplin, Mark Depristo, Joshua Dillon, and Balaji Lakshminarayanan. Likelihood ratios for out-of-distribution detection. In *Advances in Neural Information Processing Systems*, pages 14680–14691, 2019.
- Joan Serra, David Álvarez, Vicenç Gómez, Olga Slizovskaia, José F. Núñez, and Jordi Luque. Input complexity and out-of-distribution detection with likelihood-based generative models. In *International Conference on Learning Representations*, 2020.
- Kumar Sricharan and Ashok Srivastava. Building robust classifiers through generation of confident out of distribution examples. *arXiv preprint arXiv:1812.00239*, 2018.
- Yiyu Sun, Chuan Guo, and Yixuan Li. React: Out-of-distribution detection with rectified activations. In *Advances in Neural Information Processing Systems*, 2021.
- Alexandre B Tsybakov. *Introduction to nonparametric estimation*. Springer Science & Business Media, 2008.
- Joost Van Amersfoort, Lewis Smith, Yee Whye Teh, and Yarin Gal. Uncertainty estimation using a single deep deterministic neural network. In *International Conference on Machine Learning*, pages 9690–9700. PMLR, 2020.
- Sachin Vernekar, Ashish Gaurav, Vahdat Abdelzad, Taylor Denouden, Rick Salay, and Krzysztof Czarnecki. Out-of-distribution detection in classifiers via generation. *arXiv preprint arXiv:1910.04241*, 2019.
- Haoran Wang, Weitang Liu, Alex Bocchieri, and Yixuan Li. Can multi-label classification networks know what they don’t know? In *Thirty-Fifth Conference on Neural Information Processing Systems*, 2021.
- Pingmei Xu, Krista A Ehinger, Yinda Zhang, Adam Finkelstein, Sanjeev R Kulkarni, and Jianxiong Xiao. Turkergaze: Crowdsourcing saliency with webcam based eye tracking. *arXiv preprint arXiv:1504.06755*, 2015.

- Jingkang Yang, Kaiyang Zhou, Yixuan Li, and Ziwei Liu. Generalized out-of-distribution detection: A survey. *arXiv preprint arXiv:2110.11334*, 2021.
- Fisher Yu, Ari Seff, Yinda Zhang, Shuran Song, Thomas Funkhouser, and Jianxiong Xiao. Lsun: Construction of a large-scale image dataset using deep learning with humans in the loop. *arXiv preprint arXiv:1506.03365*, 2015.
- Sergey Zagoruyko and Nikos Komodakis. Wide residual networks. *arXiv preprint arXiv:1605.07146*, 2016.
- Bolei Zhou, Agata Lapedriza, Aditya Khosla, Aude Oliva, and Antonio Torralba. Places: A 10 million image database for scene recognition. *IEEE transactions on pattern analysis and machine intelligence*, 40(6): 1452–1464, 2017.

Supplemental Materials: Provable Guarantees for Understanding Out-of-distribution Detection

The main goal of the appendix is to give detailed proofs for the results presented in the main paper, and also provide details for the experimental results. The outline of the appendix would be as follows. In Section A, we recall the basic setting that we considered in the main paper. Next, we recall some notions and tools that we will need to present proofs. In Section B, we give detailed proof for Theorem 5 (Theorem 1 in the main paper). In Section C, we prove Proposition 6 (Proposition 2 in the main paper). Finally, in Section D, we present experiment details on individual OOD data-sets.

A Background

We start by briefly recalling the setting that we considered in the main paper. Let $\mathcal{X} = \mathbb{R}^d$ be the input or feature space. Throughout the following, we work with a tied covariance matrix Σ . Let $P_{\mathcal{X}}^{\text{out}}$ denotes the probability distribution on \mathcal{X} with the following probability density,

$$p_{\mathcal{X}}^{\text{out}}(\mathbf{x}) = \frac{1}{\sqrt{(2\pi)^d |\Sigma|}} \exp\left(-\frac{1}{2}(\mathbf{x} - \boldsymbol{\mu}_{\text{out}})^\top \Sigma^{-1}(\mathbf{x} - \boldsymbol{\mu}_{\text{out}})\right).$$

Next, let $P_{\mathcal{X}}^{\text{in}}$ be the probability distribution on \mathcal{X} with the following probability density,

$$p_{\mathcal{X}}^{\text{in}}(\mathbf{x}) = \frac{1}{k} \sum_{i=1}^k p_i(\mathbf{x}),$$

where,

$$p_i(\mathbf{x}) = \frac{1}{\sqrt{(2\pi)^d |\Sigma|}} \exp\left(-\frac{1}{2}(\mathbf{x} - \boldsymbol{\mu}_i)^\top \Sigma^{-1}(\mathbf{x} - \boldsymbol{\mu}_i)\right).$$

Next, recall that the re-scaled GEM function is defined by,

$$ES(\mathbf{x}) = \sum_{i=1}^k ES_i(\mathbf{x}),$$

where,

$$ES_i(\mathbf{x}) = \exp\left(-\frac{1}{2}(\mathbf{x} - \boldsymbol{\mu}_i)^\top \Sigma^{-1}(\mathbf{x} - \boldsymbol{\mu}_i)\right).$$

Recall that Theorem 5 (Theorem 1 in the main body) bounds,

$$D := \mathbb{E}_{\mathbf{x} \sim P_{\mathcal{X}}^{\text{in}}}(ES(\mathbf{x})) - \mathbb{E}_{\mathbf{x} \sim P_{\mathcal{X}}^{\text{out}}}(ES(\mathbf{x})), \quad (*)$$

in terms of Mahalanobis distance between $\boldsymbol{\mu}_{\text{out}}$ and $\boldsymbol{\mu}_i$. We start by setting notations and recalling definitions and tools that we need to prove Theorem 5 (Theorem 1 in the main body). Next, for the input or feature space \mathcal{X} , let \mathcal{B} denotes the Borel σ -algebra on \mathcal{X} and $P(\mathcal{X})$ denotes the set of all probability measures on $(\mathcal{X}, \mathcal{B})$. We recall the following definitions,

Definition 3 (Total variation). Let $P_1, P_2 \in P(\mathcal{X})$. The total variation(TV) is defined by,

$$\delta(P_1, P_2) = \sup_{A \in \mathcal{B}} |P_1(A) - P_2(A)|.$$

We use the following characterization of total variation (See for example [Müller, 1997] Theorem 5.4),

Lemma 4. Let $P_1, P_2 \in P(\mathcal{X})$ and let \mathcal{F} the unit ball in $L^\infty(\mathcal{X})$,

$$\mathcal{F} := \{f \in L^\infty(\mathcal{X}) \mid \|f\|_\infty \leq 1\},$$

then we have the following characterization for the total variation distance,

$$\delta(P_1, P_2) = \sup_{f \in \mathcal{F}} |\mathbb{E}_{\mathbf{x} \sim P_1} f(\mathbf{x}) - \mathbb{E}_{\mathbf{x} \sim P_2} f(\mathbf{x})|.$$

Next, recall definition of Kullback–Leibler(KL) divergence,

Definition 4 (Kullback–Leibler divergence). Let $P_1, P_2 \in P(\mathcal{X})$ be two probability measures with density functions p_1 and p_2 respectively. The Kullback–Leibler (KL) divergence is defined by,

$$KL(P_1||P_2) := \int_{\mathcal{X}} \ln\left(\frac{p_1(\mathbf{x})}{p_2(\mathbf{x})}\right)p_1(\mathbf{x})d\mathbf{x},$$

whenever the above integral is defined.

Next, recall the following standard lemma that computes KL divergence between *multivariate normal (MVN)* distributions,

Lemma 5. Let $P_1 \sim \mathcal{N}(\boldsymbol{\mu}_1, \Sigma)$ and $P_2 \sim \mathcal{N}(\boldsymbol{\mu}_2, \Sigma)$ then we have the following,

$$KL(P_1||P_2) = \frac{1}{2}((\boldsymbol{\mu}_1 - \boldsymbol{\mu}_2)^\top \Sigma^{-1}(\boldsymbol{\mu}_1 - \boldsymbol{\mu}_2)) = \frac{1}{2}d_M^2(\boldsymbol{\mu}_1, \boldsymbol{\mu}_2).$$

Next, we recall the following inequality that bounds the total variation by KL-divergence. (See for example [Tsybakov, 2008], Lemma 2.5 and Lemma 2.6)

Lemma 6 (Pinsker inequality). Let $P_1, P_2 \in P(\mathcal{X})$ then we have the following,

$$\delta(P_1, P_2) \leq \sqrt{\frac{1}{2}KL(P_1||P_2)},$$

the following version, which is useful when KL is large, is also true,

$$\delta(P_1, P_2) \leq 1 - \frac{1}{2} \exp(-KL(P_1||P_2)).$$

B Proof of the Energy Bounds

We start by proving the lower bound for D . We first prove the following lemma,

Lemma 7. For $1 \leq i \leq k$, let $\alpha_i := \frac{1}{2}d_M(\boldsymbol{\mu}_i, \boldsymbol{\mu}_{\text{out}})$ then we have the following estimate,

$$\mathbb{E}_{\mathbf{x} \sim P_{\mathcal{X}}^{\text{out}}}(ES_i(\mathbf{x})) \leq (1 - P_{\mathcal{X}}^{\text{out}}(B_{\alpha_i}(\boldsymbol{\mu}_{\text{out}}))) + \exp(-\frac{\alpha_i^2}{2})P_{\mathcal{X}}^{\text{out}}(B_{\alpha_i}(\boldsymbol{\mu}_{\text{out}})).$$

Proof. We have,

$$\mathbb{E}_{\mathbf{x} \sim P_{\mathcal{X}}^{\text{out}}}(ES_i(\mathbf{x})) = \int_{\mathbb{R}^d} ES_i(\mathbf{x})p_{\mathcal{X}}^{\text{out}}(\mathbf{x})d\mathbf{x} = \int_{B_{\alpha_i}(\boldsymbol{\mu}_{\text{out}})} ES_i(\mathbf{x})p_{\mathcal{X}}^{\text{out}}(\mathbf{x})d\mathbf{x} + \int_{B_{\alpha_i}^c(\boldsymbol{\mu}_{\text{out}})} ES_i(\mathbf{x})p_{\mathcal{X}}^{\text{out}}(\mathbf{x})d\mathbf{x}.$$

Next, for $\mathbf{x} \in B_{\alpha_i}(\boldsymbol{\mu}_{\text{out}})$, by triangle inequality and definition we have,

$$d_M(\boldsymbol{\mu}_{\text{out}}, \mathbf{x}) + d_M(\mathbf{x}, \boldsymbol{\mu}_i) \geq d_M(\boldsymbol{\mu}_{\text{out}}, \boldsymbol{\mu}_i) \implies d_M(\mathbf{x}, \boldsymbol{\mu}_i) \geq \alpha_i = \frac{1}{2}d_M(\boldsymbol{\mu}_i, \boldsymbol{\mu}_{\text{out}}).$$

So for the first term, we have,

$$\int_{B_{\alpha_i}(\boldsymbol{\mu}_{\text{out}})} ES_i(\mathbf{x})p_{\mathcal{X}}^{\text{out}}(\mathbf{x})d\mathbf{x} = \int_{B_{\alpha_i}(\boldsymbol{\mu}_{\text{out}})} \exp(-\frac{1}{2}d_M^2(\mathbf{x}, \boldsymbol{\mu}_i))p_{\mathcal{X}}^{\text{out}}(\mathbf{x})d\mathbf{x} \leq \exp(-\frac{1}{2}\alpha_i^2)P_{\mathcal{X}}^{\text{out}}(B_{\alpha_i}(\boldsymbol{\mu}_{\text{out}})).$$

For the second term, since $ES_i(\mathbf{x}) \leq 1$, we have,

$$\int_{B_{\alpha_i}^c(\boldsymbol{\mu}_{\text{out}})} ES_i(\mathbf{x})p_{\mathcal{X}}^{\text{out}}(\mathbf{x})d\mathbf{x} \leq (1 - P_{\mathcal{X}}^{\text{out}}(B_{\alpha_i}(\boldsymbol{\mu}_{\text{out}}))).$$

Putting all together we have,

$$\mathbb{E}_{\mathbf{x} \sim P_{\mathcal{X}}^{\text{out}}}(ES_i(\mathbf{x})) \leq (1 - P_{\mathcal{X}}^{\text{out}}(B_{\alpha_i}(\boldsymbol{\mu}_{\text{out}}))) + \exp(-\frac{1}{2}\alpha_i^2)P_{\mathcal{X}}^{\text{out}}(B_{\alpha_i}(\boldsymbol{\mu}_{\text{out}})),$$

and we are done. \square

Proposition 3. We have the following estimate,

$$\mathbb{E}_{\mathbf{x} \sim P_{\mathcal{X}}^{\text{out}}}(ES(\mathbf{x})) \leq \sum_{i=1}^k (1 - P_{\mathcal{X}}^{\text{out}}(B_{\alpha_i}(\boldsymbol{\mu}_{\text{out}}))) + \sum_{i=1}^k \exp(-\frac{\alpha_i^2}{2}) P_{\mathcal{X}}^{\text{out}}(B_{\alpha_i}(\boldsymbol{\mu}_{\text{out}})),$$

where, $\alpha_i := \frac{1}{2} d_M(\boldsymbol{\mu}_i, \boldsymbol{\mu}_{\text{out}})$.

Proof. The proof is a direct application of Lemma 7. \square

Corollary 3. Notice that since $P_{\mathcal{X}}^{\text{out}}(B_{\alpha_i}(\boldsymbol{\mu}_{\text{out}})) \leq 1$ we also have the following bound from Proposition 3.

$$\mathbb{E}_{\mathbf{x} \sim P_{\mathcal{X}}^{\text{out}}}(ES(\mathbf{x})) \leq \sum_{i=1}^k (1 - P_{\mathcal{X}}^{\text{out}}(B_{\alpha_i}(\boldsymbol{\mu}_{\text{out}}))) + \sum_{i=1}^k \exp(-\frac{\alpha_i^2}{2}),$$

where, $\alpha_i := \frac{1}{2} d_M(\boldsymbol{\mu}_i, \boldsymbol{\mu}_{\text{out}})$.

Next, we state and prove the following proposition that gives an upper bound for D in terms of Mahalanobis distance between in-distribution means and out-distribution mean,

Proposition 4. For $1 \leq i \leq k$, set $\alpha_i := \frac{1}{2} d_M(\boldsymbol{\mu}_i, \boldsymbol{\mu}_{\text{out}})$. We have the following,

$$\mathbb{E}_{\mathbf{x} \sim P_{\mathcal{X}}^{\text{in}}}(ES(\mathbf{x})) - \mathbb{E}_{\mathbf{x} \sim P_{\mathcal{X}}^{\text{out}}}(ES(\mathbf{x})) \leq \sum_{i=1}^k \alpha_i.$$

Proof. First, notice that, for $1 \leq i \leq k$,

$$ES_i(\mathbf{x}) \in [0, 1] \implies ES(\mathbf{x}) \in [0, k].$$

Therefore, by Lemma 4, we have,

$$\mathbb{E}_{\mathbf{x} \sim P_{\mathcal{X}}^{\text{in}}}(ES(\mathbf{x})) - \mathbb{E}_{\mathbf{x} \sim P_{\mathcal{X}}^{\text{out}}}(ES(\mathbf{x})) \leq k \cdot \delta(P_{\mathcal{X}}^{\text{in}}, P_{\mathcal{X}}^{\text{out}}).$$

Next, recall,

$$p_{\mathcal{X}}^{\text{in}}(\mathbf{x}) = \frac{1}{k} \sum_{i=1}^k p_i(\mathbf{x}),$$

therefore, let P_i denotes the probability distribution correspond to p_i and by triangle inequality and the definition of total variation we obtain,

$$\begin{aligned} \delta(P_{\mathcal{X}}^{\text{in}}, P_{\mathcal{X}}^{\text{out}}) &= \delta\left(\frac{1}{k} \sum_{i=1}^k P_i, P_{\mathcal{X}}^{\text{out}}\right) = \sup_{A \in \mathcal{B}} \left| \frac{1}{k} \sum_{i=1}^k P_i(A) - P_{\mathcal{X}}^{\text{out}}(A) \right| \\ &\leq \frac{1}{k} \sum_{i=1}^k \sup_{A \in \mathcal{B}} |P_i(A) - P_{\mathcal{X}}^{\text{out}}(A)| \\ &= \frac{1}{k} \sum_{i=1}^k \delta(P_i, P_{\mathcal{X}}^{\text{out}}). \end{aligned}$$

Finally, by Pinsker's inequality and Lemma 5 we have,

$$\delta(P_i, P_{\mathcal{X}}^{\text{out}}) \leq \sqrt{\frac{1}{2} KL(P_i || P_{\mathcal{X}}^{\text{out}})} = \frac{1}{2} \sqrt{(\boldsymbol{\mu}_i - \boldsymbol{\mu}_{\text{out}})^\top \Sigma^{-1} (\boldsymbol{\mu}_i - \boldsymbol{\mu}_{\text{out}})} = \frac{1}{2} d_M(\boldsymbol{\mu}_i, \boldsymbol{\mu}_{\text{out}}).$$

Putting all together we obtain,

$$\mathbb{E}_{\mathbf{x} \sim P_{\mathcal{X}}^{\text{in}}}(ES(\mathbf{x})) - \mathbb{E}_{\mathbf{x} \sim P_{\mathcal{X}}^{\text{out}}}(ES(\mathbf{x})) \leq \frac{1}{2} \sum_{i=1}^k \sqrt{(\boldsymbol{\mu}_i - \boldsymbol{\mu}_{\text{out}})^\top \Sigma^{-1} (\boldsymbol{\mu}_i - \boldsymbol{\mu}_{\text{out}})} = \frac{1}{2} \sum_{i=1}^k d_M(\boldsymbol{\mu}_i, \boldsymbol{\mu}_{\text{out}}),$$

and the proof is complete. \square

Remark 5. Proposition 4 will be useful when $d_M(\boldsymbol{\mu}_i, \boldsymbol{\mu}_{out})$ are small. Notice that when $d_M(\boldsymbol{\mu}_{out}, \boldsymbol{\mu}_i)$ is large then the right hand side of Proposition 4 is loose. However, in such a case we can instead use the second version of Pinsker's inequality in Lemma 6 and obtain the following,

$$\mathbb{E}_{\mathbf{x} \sim P_{\mathcal{X}}^{\text{in}}}(ES(\mathbf{x})) - \mathbb{E}_{\mathbf{x} \sim P_{\mathcal{X}}^{\text{out}}}(ES(\mathbf{x})) \leq k - \frac{1}{2} \sum_{i=1}^k \exp(-2\alpha_i^2).$$

The proof would be similar to the proof of Proposition 4.

Finally we combine all we proved above in the following theorem ,

Theorem 5. We have the following bounds,

- $\mathbb{E}_{\mathbf{x} \sim P_{\mathcal{X}}^{\text{out}}}(ES(\mathbf{x})) \leq \sum_{i=1}^k \left((1 - P_{\mathcal{X}}^{\text{out}}(B_{\alpha_i}(\boldsymbol{\mu}_{out}))) + \exp(-\frac{1}{2}\alpha_i^2) \right),$
- $\mathbb{E}_{\mathbf{x} \sim P_{\mathcal{X}}^{\text{in}}}(ES(\mathbf{x})) - \mathbb{E}_{\mathbf{x} \sim P_{\mathcal{X}}^{\text{out}}}(ES(\mathbf{x})) \leq \sum_{i=1}^k \alpha_i.$

where , $\alpha_i := \frac{1}{2}d_M(\boldsymbol{\mu}_i, \boldsymbol{\mu}_{out})$ for $1 \leq i \leq k$.

Proof. The first bound follows from Corollary 3 and the second bound follows from Proposition 4. □

Corollary 4. Let $\boldsymbol{\mu}_{out} = \mathbf{0} \in \mathbb{R}^d$ and $\boldsymbol{\mu}_i$ with the configuration that we considered in Section 4 of the main body and let $\Sigma = \mathbf{I}_d$. It follows that $\alpha = d_M(\boldsymbol{\mu}_{out}, \boldsymbol{\mu}_i)$ for all $1 \leq i \leq k$. We have the following from the first bound in the Theorem 5,

$$\mathbb{E}_{\mathbf{x} \sim P_{\mathcal{X}}^{\text{out}}}(ES(\mathbf{x})) \leq k \left((1 - P_{\mathcal{X}}^{\text{out}}(B_{\alpha}(\boldsymbol{\mu}_{out}))) + \exp(-\frac{1}{2}\alpha^2) \right).$$

Now as $\alpha \rightarrow \infty$ the right hand side in the above approaches to 0. This shows that the performance of GEM becomes better as $\alpha \rightarrow \infty$. On the other hand, we have the following from second part of Theorem 5,

$$\mathbb{E}_{\mathbf{x} \sim P_{\mathcal{X}}^{\text{in}}}(ES(\mathbf{x})) - \mathbb{E}_{\mathbf{x} \sim P_{\mathcal{X}}^{\text{out}}}(ES(\mathbf{x})) \leq k\alpha,$$

and it follows that as $\alpha \rightarrow 0$ the energy difference between in-distribution and out-distribution data converges to 0. In other words, the performance of GEM decreases as α approaches to 0.

C Other Proofs

Performance of our method with respect to the number of classes In this section, we work in the setting same as Section 4 from the main paper. Recall that, $\boldsymbol{\mu}_{out} = \mathbf{0} \in \mathbb{R}^d$ and $\Sigma = \mathbf{I}_d$ and $\boldsymbol{\mu}_i$ are such that for $i, j \in \{1, \dots, k\}$ and $i \neq j$,

$$\begin{aligned} \|\boldsymbol{\mu}_i - \boldsymbol{\mu}_j\| &= \sqrt{2}\alpha, \\ \|\boldsymbol{\mu}_i - \boldsymbol{\mu}_{out}\| &= \alpha. \end{aligned}$$

We compute D , defined by *, in terms of k to see how it is related to the number of classes. First, we need the following definition,

Definition 5. Let $\boldsymbol{\mu}, \boldsymbol{\nu} \in \mathbb{R}^d$ with $\|\boldsymbol{\mu} - \boldsymbol{\nu}\| = \gamma$. Let $P \sim \mathcal{N}(\boldsymbol{\mu}, \mathbf{I}_d)$. Define,

$$A_{\gamma} := \mathbb{E}_{\mathbf{x} \sim P}(\exp(-\frac{1}{2}\|\mathbf{x} - \boldsymbol{\nu}\|^2)).$$

Remark 6. Notice that A_{γ} only depends on the distance between $\boldsymbol{\mu}$ and $\boldsymbol{\nu}$ (i.e. γ). Also it is easy to see that A_{γ} decreases as γ increases.

Next, we state and prove the following proposition,

Proposition 6. We have the following,

$$D = A_0 - A_{\alpha} + (k-1)(A_{\sqrt{2}\alpha} - A_{\alpha})$$

Proof. First, recall from * that,

$$D = \mathbb{E}_{\mathbf{x} \sim P_{\mathcal{X}}^{\text{in}}}(ES(\mathbf{x})) - \mathbb{E}_{\mathbf{x} \sim P_{\mathcal{X}}^{\text{out}}}(ES(\mathbf{x})).$$

Next, for the first term we have,

$$\begin{aligned} \mathbb{E}_{\mathbf{x} \sim P_{\mathcal{X}}^{\text{in}}}(ES(\mathbf{x})) &= \sum_{i=1}^k \mathbb{E}_{\mathbf{x} \sim P_{\mathcal{X}}^{\text{in}}}(ES_i(\mathbf{x})) = \frac{1}{k} \sum_{i=1}^k \sum_{j=1}^k \mathbb{E}_{\mathbf{x} \sim P_j}(ES_i(\mathbf{x})) = \frac{1}{k} (kA_0 + k(k-1)A_{\sqrt{2}\alpha}) \\ &= A_0 + (k-1)A_{\sqrt{2}\alpha}. \end{aligned} \quad (\text{I})$$

For the second term we have,

$$\mathbb{E}_{\mathbf{x} \sim P_{\mathcal{X}}^{\text{out}}}(ES(\mathbf{x})) = \sum_{i=1}^k \mathbb{E}_{\mathbf{x} \sim P_{\mathcal{X}}^{\text{out}}}(ES_i(\mathbf{x})) = kA_{\alpha}. \quad (\text{II})$$

The result follows by combining I and II. \square

Corollary 5. *Since $\sqrt{2}\alpha > \alpha$ it follows from Remark 6 that $A_{\sqrt{2}\alpha} < A_{\alpha}$. This means that the last term term in the following is negative,*

$$D = A_0 - A_{\alpha} + (k-1)(A_{\sqrt{2}\alpha} - A_{\alpha}),$$

In other words, as k increases D becomes smaller which indicates that the performance decreases.

D Experiment Details

All experiments ran with PyTorch and NVIDIA GeForce RTX 2080Ti. The pre-trained models are downloaded from the codebase: https://github.com/wetliu/energy_ood.

Dataset		FPR95	AUROC	AUPR
\mathcal{D}_{out}^{test}		↓	↑	↑
Texture	Softmax score [Hendrycks and Gimpel, 2017]	59.28	88.50	97.16
	Energy score [Liu et al., 2020]	52.79	85.22	95.41
	ODIN [Liang et al., 2018]	49.12	84.97	95.28
	Mahalanobis [Lee et al., 2018b]	15.14	97.32	99.41
	GEM (ours)	15.06	97.33	99.41
SVHN	Softmax score [Hendrycks and Gimpel, 2017]	48.49	91.89	98.27
	Energy score [Liu et al., 2020]	35.59	90.96	97.64
	ODIN [Liang et al., 2018]	33.55	91.96	98.00
	Mahalanobis [Lee et al., 2018b]	12.86	97.59	99.47
	GEM (ours)	13.42	97.59	99.47
Places365	Softmax score [Hendrycks and Gimpel, 2017]	59.48	88.20	97.10
	Energy score [Liu et al., 2020]	40.14	89.89	97.30
	ODIN [Liang et al., 2018]	57.40	84.49	95.82
	Mahalanobis [Lee et al., 2018b]	68.42	84.41	96.08
	GEM (ours)	68.03	84.44	96.11
LSUN-C	Softmax score [Hendrycks and Gimpel, 2017]	30.80	95.65	99.13
	Energy score [Liu et al., 2020]	8.26	98.35	99.66
	ODIN [Liang et al., 2018]	15.52	97.04	99.33
	Mahalanobis [Lee et al., 2018b]	39.47	94.09	98.80
	GEM (ours)	39.46	94.13	98.81
LSUN Resize	Softmax score [Hendrycks and Gimpel, 2017]	52.15	91.37	98.12
	Energy score [Liu et al., 2020]	27.58	94.24	98.67
	ODIN [Liang et al., 2018]	26.62	94.57	98.77
	Mahalanobis [Lee et al., 2018b]	42.07	93.29	98.61
	GEM (ours)	42.89	93.27	98.61
iSUN	Softmax score [Hendrycks and Gimpel, 2017]	56.03	89.83	97.74
	Energy score [Liu et al., 2020]	33.68	92.62	98.27
	ODIN [Liang et al., 2018]	32.05	93.50	98.54
	Mahalanobis [Lee et al., 2018b]	43.80	92.75	98.46
	GEM (ours)	44.41	92.60	98.42

Table 2: OOD Detection performance of CIFAR-10 as in-distribution for each OOD test dataset. The reported results for benchmarks other than GEM are courtesy of [Liu et al., 2020]

Dataset		FPR95	AUROC	AUPR
\mathcal{D}_{out}^{test}		↓	↑	↑
Texture	Softmax score [Hendrycks and Gimpel, 2017]	83.29	73.34	92.89
	Energy score [Liu et al., 2020]	79.41	76.28	93.63
	ODIN [Liang et al., 2018]	79.27	73.45	92.75
	Mahalanobis [Lee et al., 2018b]	39.66	90.79	97.82
	GEM (ours)	39.77	90.93	97.86
SVHN	Softmax score [Hendrycks and Gimpel, 2017]	84.59	71.44	92.93
	Energy score [Liu et al., 2020]	85.82	73.99	93.65
	ODIN [Liang et al., 2018]	84.66	67.26	91.38
	Mahalanobis [Lee et al., 2018b]	43.93	90.52	97.84
	GEM (ours)	43.87	90.49	97.83
Places365	Softmax score [Hendrycks and Gimpel, 2017]	82.84	73.78	93.29
	Energy score [Liu et al., 2020]	80.56	75.44	93.45
	ODIN [Liang et al., 2018]	87.88	71.63	92.56
	Mahalanobis [Lee et al., 2018b]	90.12	68.44	91.21
	GEM (ours)	90.43	68.15	91.08
LSUN-C	Softmax score [Hendrycks and Gimpel, 2017]	66.54	83.79	96.35
	Energy score [Liu et al., 2020]	35.32	93.53	98.62
	ODIN [Liang et al., 2018]	55.55	87.73	97.22
	Mahalanobis [Lee et al., 2018b]	98.47	60.23	90.32
	GEM (ours)	98.31	60.03	90.22
LSUN Resize	Softmax score [Hendrycks and Gimpel, 2017]	82.42	75.38	94.06
	Energy score [Liu et al., 2020]	79.47	79.23	94.96
	ODIN [Liang et al., 2018]	71.96	81.82	95.65
	Mahalanobis [Lee et al., 2018b]	33.35	93.74	98.64
	GEM (ours)	33.13	93.82	98.66
iSUN	Softmax score [Hendrycks and Gimpel, 2017]	82.80	75.46	94.06
	Energy score [Liu et al., 2020]	81.04	78.91	94.91
	ODIN [Liang et al., 2018]	68.51	82.69	95.80
	Mahalanobis [Lee et al., 2018b]	36.52	92.48	98.28
	GEM (ours)	36.68	92.52	98.30

Table 3: OOD Detection performance of CIFAR-100 as in-distribution for each OOD test dataset. The reported results for benchmarks other than GEM are courtesy of [Liu et al., 2020]